IEEE Access
Multidisciplinary : Rapid Review : Open Access Journal

Received November 17, 2021, accepted November 26, 2021, date of publication December 6, 2021, date of current version December 20, 2021.

Digital Object Identifier 10.1109/ACCESS.2021.3133368

Online Model-Based Fault Detection of Synchronous Generators Using Residual Analysis

ZAHRA MASOUMI[1], BIJAN MOAVENI[2], SAYED MOHAMMAD MOUSAVI GAZAFRUDI[1], AND JAWAD FAIZ[3], (Senior Member, IEEE)

[1]School of Railway Engineering, Iran University of Science and Technology, Tehran 1311416846, Iran
[2]Faculty of Electrical Engineering, Centre of Excellence for Modelling and Control of Complex Systems, K. N. Toosi University of Technology, Tehran 1969764499, Iran
[3]School of Electrical and Computer Engineering, College of Engineering, University of Tehran, Tehran 1417935840, Iran

Corresponding author: Bijan Moaveni (b.moaveni@kntu.ac.ir)

ABSTRACT In this paper, an online model-based fault detection approach based on residual analysis in synchronous generators (SGs) is presented. Two types of faults are studied in this paper: (i) reduction of the cross-sectional area of windings wires in SGs, and (ii) air-gap eccentricity. The residual vector based on the equivalent circuit (EC) parameters or state-space model of the SG is employed for fault detection. The introduced fault detection approach employs the stator and field currents and voltages, and rotor rotational speed. The main advantage of the presented method is able to be used for linear and nonlinear loads in the presence of uncertainty in EC parameters. The effectiveness of the proposed method is shown using the experimental data of five SGs in diesel-electric locomotives.

INDEX TERMS Synchronous generator, air-gap eccentricity fault, fault detection, model-based approach.

I. INTRODUCTION

Online fault detection of faulty components on time can prevent catastrophic failures of power systems. Synchronous generators (SGs) are the leading equipment for converting mechanical energy to electrical energy. SGs can be driven by hydro, steam, wind, or combustion engines, such as SGs in diesel-electric locomotives [1]–[4].

In diesel-electric locomotives, the diesel engine is used to rotate the rotor shaft of SG. The rotor rotational speed varies depending on the amount of required power or modes of train movement such as service mode and acceleration mode [5], [6].

Faults in SGs can be divided into two main parts: rotor faults and stator faults. Rotor eccentricity, rotor bending, inter-turn short circuit, and inter-slot short circuit are the primary faults in the rotor. Multi-phase short circuit, single-phase short circuit, inter-turn short circuit, and saturation are the primary faults in the stator [7], [8]. Also, a reduction of the cross-sectional area of windings wires is a fault that can be occurred in both stator and rotor (field and damper) windings. Electrical, thermal, and mechanical stresses are the main reasons for damaging winding insulation, reducing the cross-sectional area of windings wires, and ultimately disconnection in windings of SGs [9].

Model-based fault detection approaches are used when the system models in healthy and faulty conditions are available [10]. A brief review of various methods for modeling of SGs has been presented in [8]. A model-based fault detection methodology has been used to diagnose air-gap eccentricity and inter-turn short circuits in the SG [11], [12]. In [13] and [14], a model for an SG with dynamic eccentricity fault using modified winding function theory has been presented. Faiz *et al.* [11] have introduced a method based on the winding function to calculate the self-inductance of stator and rotor, the mutual inductance of the two phases of the stator, and mutual inductance of the rotor and stator under static and dynamic eccentricities. Also, in [11], an online model-based approach has been introduced for mixed static and dynamic eccentricity fault diagnosis by using the winding function method.

The associate editor coordinating the review of this manuscript and approving it for publication was Baoping Cai.

A number of researches have been done regarding the inter-turn short circuit faults. The inter-turn short circuit models of field winding have been introduced in [15], [16]. Hao *et al.* [15] have presented an online monitoring approach for inter-turn short circuits in the field winding of SGs based on the mathematical model. Wang *et al.* [12] have introduced a fault diagnosis method for an inter-turn short circuit in the rotor windings based on Volterra kernel identification. Since loads of SG have affected the stator voltages and currents, an approach based on an analytical redundancy relationship has been introduced in [17] to recognize the external faults from internal faults in SGs. Also, Vilchis-Rodriguez *et al.* [18] have introduced a model of the internal fault in SGs based on the voltage-behind-reactance representation.

In some studies, by describing SGs faults as additive faults in general, fault detection methods based on an observer and residual analysis for power systems have been presented [19], [20]. In [19] and [20], by defining the stator voltages as sinusoidal waveforms, the residual vector and the detection threshold have been extracted.

Another set of fault detection methodologies are signal-based. In these methods, instead of the model of SG, a database of all possible operating points in healthy and faulty conditions is required. Eccentricity fault, inter-turn short circuit fault, ground-fault, field winding, phase-phase/3-phase fault, and phase-ground faults are some consideration faults to present fault detection techniques [21]–[31]. Biet [21] has introduced a signal-based method based on the signals analysis of flux probes and classical electric measurements for rotor faults diagnosis. In the experimental part of [21], eccentricity fault and inter-turn short circuit fault were considered. Bruzzese [22] employed a combined space-vector and fast Fourier transformation analysis for eccentricity fault diagnosis. Gyftakis *et al.* [23] introduced a method for static eccentricity fault diagnosis by using stator currents. In [24] and [25], two methods for detecting inter-turn short circuits of rotor windings were proposed. Fault detection based on frequency analysis is one of the signal-based methods used to detect the ground-fault and field winding fault [26], [27]. Furthermore, Pardo *et al.* [28] have presented an online method for the detection and location of a ground fault. Doorwar *et al.* [29] have introduced a technique to an inter-turn fault, phase-phase/3-phase fault, and phase-ground faults as internal faults detection.

In the above signal-based techniques, loads of SGs have been modeled as resistance or inductance. If the load of SG has a nonlinear model, such as traction motors in diesel-electric locomotives, the above methods are not working properly. Consequently, in this paper, a model-based approach based on the residual vector is introduced for online fault detection of two types of faults in SGs: (i) reduction of the cross-sectional area of wires in windings and (ii) air-gap eccentricity. A reduction of the cross-sectional area of windings wires leads to a thinner conductor of the stator and, or rotor (field and damper) windings. Air-gap eccentricity faults are classified as static, dynamic, and mixed eccentricity. The equivalent circuit (EC) parameters or state-space model of SG are required to extract the residual vector. Online fault detection of SGs under linear or nonlinear load by considering the uncertainty of nominal EC parameters is the main advantage of this method. The validation process is done by using the experimental data of five SGs used in five diesel-electric locomotives.

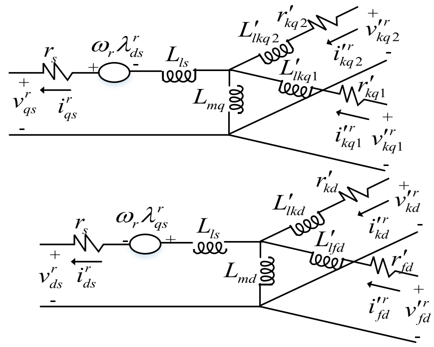

FIGURE 1. EC of a three-phase SG in the rotor reference frame referred to the stator [1].

The paper is organized as follows: in section II, the state-space models of SG in healthy and faulty conditions are introduced. In section III, the faults detection based on residual vector is presented. In section IV, the experimental results are presented to validate the proposed approach. Section V concludes the paper.

II. STATE-SPACE MODEL OF SYNCHRONOUS GENERATOR

SGs based on the structure of field windings are classified into two types: salient pole and non-salient pole. In this section, the state-space model of a three-phase salient-pole SG with three damper windings is presented in healthy and faulty conditions.

A. HEALTHY MODEL

EC of a three-phase SG with three damper windings in the rotor reference frame is shown in Figure 1. According to the EC of three-phase an SG, its dynamic equations for $v_{qs}^r, v_{ds}^r, v'^r_{kq1}, v'^r_{kq2}, v'^r_{fd}$, and v'^r_{kd} are presented as (1) [1].

$$\begin{aligned} v_{qs}^r(t) = &-r_s i_{qs}^r(t) - \omega_r(t)\left(L_{ls} + L_{md}\right) i_{ds}^r(t) \\ &+\omega_r(t) L_{md} i'^r_{fd}(t) \\ &+\omega_r L_{md} i'^r_{kd}(t) - \left(L_{ls} + L_{mq}\right)\frac{di_{qs}^r(t)}{dt} \\ &+L_{mq}\frac{di'^r_{kq1}(t)}{dt} \\ &+L_{mq}\frac{di'^r_{kq2}(t)}{dt} \end{aligned} \tag{1a}$$

$$v_{ds}^{r}(t) = -r_s i_{ds}^{r}(t) + \omega_r(t)\left(L_{ls}+L_{mq}\right) i_{qs}^{r}(t) - \omega_r(t) L_{mq} i'^{r}_{kq1}(t) - \omega_r(t) L_{mq} i'^{r}_{kq2}(t) + L_{md}\frac{di'^{r}_{fd}(t)}{dt} + L_{md}\frac{di'^{r}_{kd}(t)}{dt} - \left(L_{ls}+L_{md}\right)\frac{di_{ds}^{r}(t)}{dt} \tag{1b}$$

$$v'^{r}_{kq1}(t) = \left(L'_{lkq1}+L_{mq}\right)\frac{di'^{r}_{kq1}(t)}{dt} + L_{mq}\frac{di'^{r}_{kq2}(t)}{dt} - L_{mq}\frac{di_{qs}^{r}(t)}{dt} + r'_{kq1} i'^{r}_{kq1}(t) \tag{1c}$$

$$v'^{r}_{kq2}(t) = \left(L'_{lkq2}+L_{mq}\right)\frac{di'^{r}_{kq2}(t)}{dt} + L_{mq}\frac{di'^{r}_{kq1}(t)}{dt} - L_{mq}\frac{di_{qs}^{r}(t)}{dt} + r'_{kq2} i'^{r}_{kq2}(t) \tag{1d}$$

$$v'^{r}_{fd}(t) = \left(L'_{lfd}+L_{md}\right)\frac{di'^{r}_{fd}(t)}{dt} - L_{md}\frac{di_{ds}^{r}(t)}{dt} + L_{md}\frac{di'^{r}_{kd}(t)}{dt} + r'_{fd} i'^{r}_{fd}(t) \tag{1e}$$

$$v'^{r}_{kd}(t) = \left(L'_{lkd}+L_{md}\right)\frac{di'^{r}_{kd}(t)}{dt} - L_{md}\frac{di_{ds}^{r}(t)}{dt} + L_{md}\frac{di'^{r}_{fd}(t)}{dt} + r'_{kd} i'^{r}_{kd}(t) \tag{1f}$$

where, r_s and L_{ls} are the stator resistance and leakage inductance, respectively. r'_{fd}, r'_{kd}, r'_{kq1}, and r'_{kq2} are the field and damper windings resistances referred to the stator, respectively. L'_{lfd}, L'_{lkd}, L'_{lkq1}, and L'_{lkq2} are the leakage inductances of the field and damper windings referred to the stator, respectively. L_{md} and L_{mq} are the magnetizing inductances in the dq-axes. $i_{ds}^{r}(t)$, $i_{qs}^{r}(t)$, $i'^{r}_{fd}(t)$, $i'^{r}_{kd}(t)$, $i'^{r}_{kq1}(t)$, and $i'^{r}_{kq2}(t)$ are the stator, field, and damper winding currents in the dq-axes rotor reference frame referred to the stator, respectively. $\lambda_{ds}^{r}(t)$ and $\lambda_{qs}^{r}(t)$ are the stator flux linkages in the dq rotor reference frame, and $\omega_r(t)$ is the rotor rotational speed.

By defining the state, input, and output variables as (2) -(4), as shown at the bottom of the page, the state-space model of the SG in the continuous-time domain is defined as (5), as shown at the bottom of the page. In (5), N_s and N_{fd} are equivalent turns of stator and field winding, respectively, $n_d = 3$ is the number of damper winding and $\mathbf{J}_{n_1\times n_2}$ is an all-ones matrix.

Clearly, L_{ls}, L'_{lkq1}, L'_{lkq2}, L'_{lfd}, L'_{lkd}, L_{md}, and L_{mq} in SGs have positive values, therefore using (5i), (6) and for $n_d = 3$, we can show that $\mathbf{L}$ is a nonsingular matrix.

$$\begin{aligned}\det(\mathbf{L}) = {} & L'_{lfd}L_{ls}^2(L'_{lkq1}L'_{lkq2}(L'_{lkd}+L_{md}) + L_{mq}(L'_{lkd}L'_{lkq2}+L'_{lkq1}L_{md})) + L'_{lfd}L'_{lkd} \\ & (L'_{lkq1}L'_{lkq2}(L_{ls}(L_{md}+L_{mq})+L_{md}L_{mq}) + L_{ls}L_{md} \\ & L_{mq}(L'_{lkq1}+L'_{lkq2})) + L'_{lkd}L'_{lkq1}L_{ls}^2(L'_{lkq2}L_{md} \\ & + L'_{lfd}L_{mq}) + L'_{lkq1}L'_{lkq2}L_{ls}L_{md}L_{mq} \\ & (L'_{lfd}+L'_{lkd}) + L_{ls}^2 L_{md}L_{mq}(L'_{lkq2}(L'_{lfd}+L'_{lkd}) \\ & + L'_{lkd}L'_{lkq1}) \neq 0\end{aligned} \tag{6}$$

$$\mathbf{x_c}(t) = \left[x_{c_i}(t)\right]_{6\times1} = \left[\, i_{qs}^{r}(t) \quad i_{ds}^{r}(t) \quad i'^{r}_{kq1}(t) \quad i'^{r}_{kq2}(t) \quad i'^{r}_{fd}(t) \quad i'^{r}_{kd}(t) \,\right]^T \tag{2}$$

$$\tilde{\mathbf{u}}_{\mathbf{c}}(t) = \left[\, v_{qs}^{r}(t) \quad v_{ds}^{r}(t) \quad v'^{r}_{kq1}(t) \quad v'^{r}_{kq2}(t) \quad v_{fd}^{r}(t) \quad v'^{r}_{kd}(t) \,\right]^T \tag{3}$$

$$\tilde{\mathbf{y}}_{\mathbf{c}}(t) = \left[\, i_{qs}^{r}(t) \quad i_{ds}^{r}(t) \quad i_{fd}^{r}(t) \,\right]^T \tag{4}$$

$$\begin{cases}\dot{\mathbf{x}}_{\mathbf{c}}(t) = \mathbf{A_c}(\omega_r(t))\mathbf{x_c}(t) + \mathbf{B_c}\tilde{\mathbf{u}}_{\mathbf{c}}(t)\\ \tilde{\mathbf{y}}_{\mathbf{c}}(t) = \mathbf{C_c}\mathbf{x_c}(t)\end{cases} \tag{5a}$$

$$\mathbf{A_c}(\omega_r(t)) = \left(\mathbf{A_{c_1}} + \omega_r(t)\mathbf{A_{c_2}}\right) \tag{5b}$$

$$\mathbf{A_{c_1}} = -\mathbf{L}^{-1}\mathbf{R}_{c_1} = \left[a_{1_{ij}}\right]; \quad i,j = 1,\ldots,6 \tag{5c}$$

$$\mathbf{A_{c_2}} = -\mathbf{L}^{-1}\left[\,\mathbf{R}_{c_2}^T \quad \mathbf{0}_{6\times4}\,\right]^T = \left[a_{2_{ij}}\right]; \quad i,j = 1,\ldots,6 \tag{5d}$$

$$\mathbf{B_c} = \mathbf{L}^{-1}\begin{bmatrix}\mathbf{I}_{(1+n_d)\times(1+n_d)} & \mathbf{0}_{(1+n_d)\times2}\\ \mathbf{0}_{2\times(1+n_d)} & \begin{bmatrix}(N_s/N_{fd}) & 0\\ 0 & 1\end{bmatrix}\end{bmatrix} \tag{5e}$$

$$\mathbf{C_c} = \begin{bmatrix}\mathbf{I}_{2\times2} & \mathbf{0}_{2\times(n_d-1)} & \mathbf{0}_{2\times1} & \mathbf{0}_{2\times1}\\ \mathbf{0}_{1\times2} & \mathbf{0}_{1\times(n_d-1)} & (3N_s/2N_{fd}) & 0\end{bmatrix} \tag{5f}$$

$$\mathbf{R}_{c_1} = diag\left(-r_s, -r_s, r'_{kq1}, r'_{kq2}, \ldots, r'_{kq(n_d-1)}, r'_{fd}, r'_{kd}\right) \tag{5g}$$

$$\mathbf{R}_{c_2} = \begin{bmatrix}0 & -\left(L_{ls}+L_{md}\right) & \mathbf{0}_{1\times(n_d-1)} & L_{md} & L_{md}\\ \left(L_{ls}+L_{mq}\right) & 0 & -L_{mq}\mathbf{J}_{1\times(n_d-1)} & 0 & 0\end{bmatrix} \tag{5h}$$

$$\mathbf{L} = \begin{bmatrix}-\left(L_{ls}+L_{mq}\right) & 0 & L_{mq}\mathbf{J}_{1\times(n_d-1)} & \mathbf{0}_{1\times2}\\ 0 & -\left(L_{ls}+L_{md}\right) & \mathbf{0}_{1\times(n_d-1)} & L_{md}\mathbf{J}_{1\times2}\\ -L_{mq}\mathbf{J}_{(n_d-1)\times1} & \mathbf{0}_{(n_d-1)\times1} & \mathbf{L_1} & \mathbf{0}_{(n_d-1)\times2}\\ \mathbf{0}_{2\times1} & -L_{md}\mathbf{J}_{2\times1} & \mathbf{0}_{2\times(n_d-1)} & \mathbf{L}_2\end{bmatrix} \tag{5i}$$

$$\mathbf{L_1} = L_{mq}\mathbf{J}_{(n_d-1)\times(n_d-1)} + diag\left(L'_{lkq1}, L'_{lkq2}, \ldots, L'_{lkq(n_d-1)}\right) \tag{5j}$$

$$\mathbf{L}_2 = L_{md}\mathbf{J}_{2\times2} + diag\left(L'_{lfd}, L'_{lkd}\right) \tag{5k}$$

Please note that the state-space model of an SG in (5) can be easily extended to the non-salient pole SG or an SG with a different number of damper windings. It is well known that in a non-salient pole SG $L_{mq} = L_{md}$. Also, in an SG with n_d damper windings, kqi; $i = 1, \ldots, n_d - 1, kd$, the order of the state-space model in (5) will be equal to $(n_d + 3)$.

B. FALTY MODELS

In this section, the state-space models of SGs are presented in two faulty cases: (i) A reduction of the cross-sectional area of wires in windings, (ii) Air-gap eccentricity.

1) A REDUCTION OF THE CROSS-SECTIONAL AREA OF WINDINGS WIRES

Evidently, the cross-sectional area decreasing of wires before disconnection leads to an increase in the resistance of windings. By considering the state-space model of SGs, (5), the resistance of windings has an effect on $\mathbf{A_{c_1}}$, (5c), and (5g). Therefore, the effect of reduction of the cross-sectional area of windings wires on the state matrix is defined as $\mathbf{A_{c}}_{f_{11}}$, (7).

$$\mathbf{A_{c}}_{f_{11}} = \mathbf{A_{c_1}} + \mathbf{F_{c_1}} \tag{7}$$

where

$$\mathbf{F_{c_1}} = -\mathbf{L}^{-1} diag(-r_{dis_s}, -r_{dis_s}, r'_{dis_{kq1}}, r'_{dis_{kq2}}, r'_{dis_{fd}}, r'_{dis_{kd}}) \tag{8}$$

r_{dis_s}, $r'_{dis_{fd}}$, $r'_{dis_{kq1}}$, $r'_{dis_{kq2}}$, and $r'_{dis_{kd}}$ are the increased resistance values of the stator, field, and damper windings, respectively. Also, the additive faults vector in this condition can be defined as $\mathbf{f_{c_1}}(t)$, (9).

$$\mathbf{f_{c_1}}(t) = \mathbf{F_{c_1}} \mathbf{x_c}(t) = \left[f_{1_i}(t)\right]; \quad i = 1, \ldots, 6 \tag{9}$$

2) AIR-GAP ECCENTRICITY

Three types of eccentricity (static, dynamic, and mixed) can occur in SGs. In the static eccentricity, the rotation axis of the rotor does not coincide with the stator axis of symmetry. In the dynamic eccentricity, the rotation axis of the rotor coincides with the stator axis of symmetry, but the rotor axis symmetry is displaced. In the mixed eccentricity, static and dynamic eccentricities are occurred simultaneously [14]. Therefore, eccentricity faults lead to change in the maximum and minimum length of the air gap. By defining m_1 and m_2 as the maximum and minimum length of air-gap, respectively, L_{md} and L_{mq} are defined as follows [32]:

$$L_{md} = (3/2)\,(L_A + L_B) \tag{10}$$
$$L_{mq} = (3/2)\,(L_A - L_B) \tag{11}$$

where,

$$L_A = (N_s/2\sqrt{2})^2 \pi \mu_0 r l \,((1/m_1) + (1/m_2)) \tag{12}$$
$$L_B = (N_s/4)^2 \pi \mu_0 r l((1/m_2) - (1/m_1)) \tag{13}$$

μ_0 is the permeability of the free space, r is the air gap mean radius, l is the air gap axial length. When eccentricity fault occurs, L_{md} and L_{mq} are changed. In [11], by using the modified winding function method, the self-inductances and mutual inductances were determined in the static, dynamic, and mixed eccentricity conditions. In other words, L_{md}, L_{mq}, $(L_{mq} + L_{ls})$, $(L_{md} + L_{ls})$, $(L_{mq} + L'_{lkq1})$, $(L_{mq} + L'_{lkq2})$, $(L_{md} + L'_{lfd})$, and $(L_{md} + L'_{lkd})$ are increased in the static, dynamic, and mixed eccentricity conditions.

By considering the elements of $\mathbf{R}_{c_2}$ and $\mathbf{L}$ in (5h(-)5i), if the eccentricity faults have occurred, then these two matrices are changed to $(\mathbf{R}_{c_2} + \mathbf{R}_{cf_2})$ and $(\mathbf{L} + \mathbf{L}_f)$, respectively. Elements of $\mathbf{R}_{cf_2}$ and $\mathbf{L}_f$ are the amount of increase in the inductances. Therefore, $\mathbf{A_{c_1}}$, $\mathbf{A_{c_2}}$, and $\mathbf{B_c}$ in faulty cases are defined as follows:

$$\begin{aligned}\mathbf{A_c}_{f_{12}} &= -(\mathbf{L} + \mathbf{L}_f)^{-1}\mathbf{R}_{c_1}\\ &= -(\mathbf{L}^{-1} - \mathbf{L}^{-1}\mathbf{L}_f(\mathbf{L}^{-1}\mathbf{L}_f + \mathbf{I})^{-1}\mathbf{L}^{-1})\mathbf{R}_{c_1}\\ &= \mathbf{A_{c_1}} + \mathbf{F_{c_{21}}}\end{aligned} \tag{14}$$

$$\begin{aligned}\mathbf{A_c}_{f_{22}} &= -\left(\mathbf{L} + \mathbf{L}_f\right)^{-1}\left[\left(\mathbf{R}_{c_2} + \mathbf{R}_{cf_2}\right)^T \ \mathbf{0}_{6\times 4}\right]^T\\ &= \mathbf{A_{c_2}} + \mathbf{F_{c_{22}}}\end{aligned} \tag{15}$$

$$\begin{aligned}\mathbf{B_c}_{f_2} &= \left(\mathbf{L} + \mathbf{L}_f\right)^{-1}\begin{bmatrix}\mathbf{I}_{4\times 4} & \mathbf{0}_{4\times 2}\\ \mathbf{0}_{2\times 4} & \begin{bmatrix}(N_s/N_{fd}) & 0\\ 0 & 1\end{bmatrix}\end{bmatrix}\\ &= \mathbf{B_c} + \mathbf{F_{c_{23}}}\end{aligned} \tag{16}$$

where,

$$\mathbf{F_{c_{21}}} = (\mathbf{L}^{-1}\mathbf{L}_f(\mathbf{L}^{-1}\mathbf{L}_f + \mathbf{I})^{-1}\mathbf{L}^{-1})\mathbf{R}_{c_1} \tag{17}$$

$$\begin{aligned}\mathbf{F_{c_{22}}} &= -\mathbf{L}^{-1}\begin{bmatrix}\mathbf{R}_{cf_2}\\ \mathbf{0}_{4\times 6}\end{bmatrix} + \left(\mathbf{L}^{-1}\mathbf{L}_f\left(\mathbf{L}^{-1}\mathbf{L}_f + \mathbf{I}\right)^{-1}\mathbf{L}^{-1}\right)\\ &\quad\times\begin{bmatrix}\mathbf{R}_{c_2} + \mathbf{R}_{cf_2}\\ \mathbf{0}_{4\times 6}\end{bmatrix}\end{aligned} \tag{18}$$

$$\begin{aligned}\mathbf{F_{c_{23}}} &= \left(-\mathbf{L}^{-1}\mathbf{L}_f\left(\mathbf{L}^{-1}\mathbf{L}_f + \mathbf{I}\right)^{-1}\mathbf{L}^{-1}\right)\\ &\quad\times\begin{bmatrix}\mathbf{I}_{4\times 4} & \mathbf{0}_{4\times 2}\\ \mathbf{0}_{2\times 4} & \begin{bmatrix}(N_s/N_{fd}) & 0\\ 0 & 1\end{bmatrix}\end{bmatrix}\end{aligned} \tag{19}$$

Therefore, the additive fault vector, $\mathbf{f_{c_2}}(t)$, is defined as follows:

$$\mathbf{f_{c_2}}(t) = (\mathbf{F_{c_{21}}} + \omega_r(t)\mathbf{F_{c_{22}}})\mathbf{x_c}(t) + \mathbf{F_{c_{23}}}\tilde{\mathbf{u}}_\mathbf{c}(t) = \left[f_{2_i}(t)\right]; \quad i = 1, \ldots, 6 \tag{20}$$

Also, the state-space model of the SG in both faulty cases is defined as (21).

$$\begin{cases}\dot{\mathbf{x}}_\mathbf{c}(t) = \mathbf{A_c}(\omega_r(t))\mathbf{x_c}(t) + \mathbf{B_c}\tilde{\mathbf{u}}_\mathbf{c}(t) + \mathbf{f_c}(t)\\ \tilde{\mathbf{y}}_\mathbf{c}(t) = \mathbf{C_c}\mathbf{x_c}(t)\end{cases} \tag{21}$$

where,

$$\mathbf{f_c}(t) = \mathbf{f_{c_1}}(t) + \mathbf{f_{c_2}}(t) = (\mathbf{F_{c_1}} + \mathbf{F_{c_{21}}} + \omega_r(t)\mathbf{F_{c_{22}}})\,\mathbf{x_c}(t) + \mathbf{F_{c_{23}}}\tilde{\mathbf{u}}_\mathbf{c}(t) \tag{22}$$

III. FAULT DETECTION BASED ON RESIDUAL VECTOR

In this section, a fault detection methodology for SGs based on the residual vector is introduced. The measured output vector, $\mathbf{y_c}(t)$, and measured input vector, $\mathbf{u_c}(t)$, are defined as follows:

$$\mathbf{u_c}(t) = \tilde{\mathbf{u}}_c(t) + \mathbf{v_{u_c}}(t) \tag{23a}$$
$$\mathbf{y_c}(t) = \tilde{\mathbf{y}}_\mathbf{c}(t) + \mathbf{v_{y_c}}(t) \tag{23b}$$

where $\mathbf{v_{u_c}}(t)$ and $\mathbf{v_{y_c}}(t)$ are measurement noises. Using (21), the measured output matrix, $\mathbf{Y_c}$, is obtained as follows [33]:

$$\mathbf{Y_c} = \Phi(\omega_r(t))\mathbf{x_c}(t) + \mathbf{T}_{u,3}(\omega_r(t))(\mathbf{U_c} - \mathbf{V_{u_c}}) + \mathbf{T}_{f,3}(\omega_r(t))\bar{\mathbf{f}}_\mathbf{c} + \mathbf{V_{y_c}} \tag{24}$$

where,

$$\mathbf{Y_c} = \left[\mathbf{y}_\mathbf{c}^T(t)\ \dot{\mathbf{y}}_\mathbf{c}^T(t)\ \ddot{\mathbf{y}}_\mathbf{c}^T(t)\right]^T \tag{25}$$
$$\mathbf{U_c} = \left[\mathbf{u}_\mathbf{c}^T(t)\ \dot{\mathbf{u}}_\mathbf{c}^T(t)\right]^T \tag{26}$$
$$\mathbf{V_{y_c}} = \left[\mathbf{v}_\mathbf{y_c}^T(t)\ \dot{\mathbf{v}}_\mathbf{y_c}^T(t)\ \ddot{\mathbf{v}}_\mathbf{y_c}^T(t)\right]^T \tag{27}$$
$$\mathbf{V_{u_c}} = \left[\mathbf{v}_\mathbf{u_c}^T(t)\ \dot{\mathbf{v}}_\mathbf{u_c}^T(t)\right]^T \tag{28}$$
$$\Phi(\omega_r(t)) = \left(\left[\mathbf{C}_c^T \quad (\mathbf{C_c A_c}(\omega_r(t)))^T \quad \left(\mathbf{C_c}\left(\mathbf{A}_\mathbf{c}^2(\omega_r(t)) + \dot{\omega}_r(t)\mathbf{A_{c_2}}\right)\right)^T\right]^T\right)_{9\times 6} \tag{29}$$
$$\bar{\mathbf{f}}_\mathbf{c} = \left[\mathbf{f}_\mathbf{c}^T(t)\ \dot{\mathbf{f}}_\mathbf{c}^T(t)\right]^T \tag{30}$$
$$\mathbf{T}_{u,3}(\omega_r(t)) = \begin{bmatrix} \mathbf{0}_{3\times 6} & \mathbf{0}_{3\times 6} \\ \mathbf{C_c B_c} & \mathbf{0}_{3\times 6} \\ \mathbf{C_c A_c}(\omega_r(t))\mathbf{B_c} & \mathbf{C_c B_c} \end{bmatrix} \tag{31}$$
$$\mathbf{T}_{f,3}(\omega_r(t)) = \begin{bmatrix} \mathbf{0}_{3\times 6} & \mathbf{0}_{3\times 6} \\ \mathbf{C_c} & \mathbf{0}_{3\times 6} \\ \mathbf{C_c A_c}(\omega_r(t)) & \mathbf{C_c} \end{bmatrix} \tag{32}$$

Since $\omega_r(t) \neq 0$ and the null space of $\Phi(\omega_r(t))$ is not empty, $\mathbf{W}$ can be obtained as follows:

$$\mathbf{W}\Phi(\omega_r(t)) = \mathbf{0}_{3\times 6};\ \mathbf{W} \in \mathbf{R}^{3\times 9}, \quad \mathbf{W} = [w_{ij}]; \quad i = 1, 2, 3, j = 1, \ldots, 9 \tag{33}$$

In other words, the components of $\mathbf{W}$ can be defined as follows:

$$[w_{i1}\ w_{i2}\ w_{i3}\ w_{i4}\ w_{i5}\ w_{i6}\ w_{i7}\ w_{i8}\ w_{i9}]\left[\mathbf{C}_\mathbf{c}^T\ \mathbf{H}^T\right]^T = \mathbf{0}_{9\times 6}; \quad i = 1, 2, 3 \tag{34a}$$
$$[w_{i4}\ w_{i5}\ w_{i6}\ w_{i7}\ w_{i8}\ w_{i9}] = \left[-w_{i1}\ -w_{i2}\ 0\ 0\ -(3N_s/2N_{fd})w_{i3}\ 0\right]\mathbf{H}^{-1}; \quad i = 1, 2, 3 \tag{34b}$$
$$\mathbf{H} = [h_{ij}] = \left[\varphi_4^T\ \varphi_5^T\ \varphi_6^T\ \varphi_7^T\ \varphi_8^T\ \varphi_9^T\right]^T; \quad i, j = 1, \ldots, 6 \tag{35}$$

where $h_{ij} \neq 0$ and $\varphi_i;\ i = 1, \ldots, 9$ are the rows of $\Phi(\omega_r(t))$ in (29). Based on the format of $\mathbf{C_c}$ in (5f) and (34b), w_{i1}, w_{i2}, and $w_{i3};\ i = 1, 2, 3$ must be non-zero simultaneously. Otherwise, $\mathbf{W}$ will be a zero matrix. In other words, at least one of the $w_{ij};\ i, j = 1, 2, 3$ must be non-zero. Multiplying both sides of (24) by $\mathbf{W}$ results in:

$$\mathbf{WY_c} - \mathbf{WT}_{u,3}(\omega_r(t))\mathbf{U_c} = -\mathbf{WT}_{u,3}(\omega_r(t))\mathbf{V_{u_c}} + \mathbf{WT}_{f,3}(\omega_r(t))\bar{\mathbf{f}}_\mathbf{c} + \mathbf{WV_{y_c}} \tag{36}$$

Therefore, the residual vector and decision thresholds are defined as (37) and (38), respectively.

$$\mathbf{r}(t) = \mathbf{WY_c} - \mathbf{WT}_{u,3}(\omega_r(t))\mathbf{U_c};\ \mathbf{r}(t) \in \mathbf{R}^{3\times 1} \tag{37}$$

$$\begin{cases} \mathbf{r}(t) = \mathbf{WV_{y_c}} - \mathbf{WT}_{u,3}(\omega_r(t))\mathbf{V_{u_c}}; \\ \text{if } \bar{\mathbf{f}}_\mathbf{c} = \mathbf{0} \text{ (There is no detectable fault.)} \\ \mathbf{r}(t) = \mathbf{WV_{y_c}} - \mathbf{WT}_{u,3}(\omega_r(t))\mathbf{V_{u_c}} + \mathbf{WT}_{f,3}(\omega_r(t))\bar{\mathbf{f}}_\mathbf{c}; \\ \text{if } \bar{\mathbf{f}}_\mathbf{c} \neq \mathbf{0} \text{ (There is at least a detectable fault.)} \end{cases} \tag{38}$$

Note 1: In the case that there is no air-gap eccentricity fault, $\mathbf{f}_{\mathbf{c}_2}(t) = \mathbf{0}_{6\times 1}$ and $\mathbf{f}_{\mathbf{c}_1}(t) \neq \mathbf{0}_{6\times 1}$, therefore $\mathbf{r}(t)$ in (38) can be rewritten as follows:

$$\mathbf{r}(t) = \mathbf{V}_N + \mathbf{WT}_{f,3}(\omega_r(t))\bar{\mathbf{f}}_\mathbf{c} = [r_1(t)\ r_2(t)\ r_3(t)]^T;\ \text{if } \bar{\mathbf{f}}_\mathbf{c} \neq \mathbf{0} \tag{39}$$

$$\mathbf{V}_N = \mathbf{WV_{y_c}} - \mathbf{WT}_{u,3}(\omega_r(t))\mathbf{V_{u_c}} = [v_{Ni}]; \quad i = 1, \ldots, 3 \tag{40}$$

$$\begin{aligned} r_j(t) = {} & v_{Nj} + w_{j4}f_{1_1}(t) + w_{j5}f_{1_2}(t) + w_{j6}(3N_s/2N_{fd})f_{1_5}(t) \\ & + w_{j7}\Big(\sum_{i=1}^{5} a_{1i}f_{1_i}(t) + a_{15}f_{1_6}(t) - r_{dis_s}\dot{x}_{c1}(t)\bar{L}_{11} \\ & + \dot{x}_{c3}(t)r'_{dis_{kq1}}\bar{L}_{13} + r'_{dis_{kq2}} \\ & \bar{L}_{14}\dot{x}_{c4}(t)\Big) + w_{j8}\Big(\sum_{\substack{i=1\\ i\neq 4}}^{6} a_{2i}f_{1_i}(t) + a_{23}f_{1_4}(t) \\ & - r_{dis_s}\dot{x}_{c2}(t)\bar{L}_{22} + \dot{x}_{c5}(t)r'_{dis_{fd}} \\ & \bar{L}_{25} + r'_{dis_{kd}}\bar{L}_{26}\dot{x}_{c6}(t)\Big) + w_{j9}\Big(\sum_{\substack{i=1\\ i\neq 4}}^{6} a_{5i}f_{1_i}(t) + a_{53}f_{1_4}(t) \\ & + 3N_s/2N_{fd}\Big) \\ & (-r_{dis_s}\dot{x}_{c2}(t) + \dot{x}_{c5}(t)r'_{dis_{fd}}\bar{L}_{55} + r'_{dis_{kd}}\bar{L}_{56}\dot{x}_{c6}(t))); \\ & j = 1, 2, 3 \end{aligned} \tag{41}$$

$$\begin{cases} f_{1_i}(t) = -r_{dis_s}x_{c1}(t)\bar{L}_{i1} + r'_{dis_{kq1}}x_{c3}(t)\bar{L}_{i3} + r'_{dis_{kq2}}\bar{L}_{i4}x_{c4}(t); \\ i = 1, 3, 4 \\ f_{1_i}(t) = -r_{dis_s}x_{c2}(t)\bar{L}_{i2} + r'_{dis_{fd}}x_{c5}(t)\bar{L}_{i5} + r'_{dis_{kd}}\bar{L}_{i6}x_{c6}(t); \\ i = 2, 5, 6 \end{cases} \tag{42}$$

$$\mathbf{L}^{-1} = [\bar{L}_{ij}]; \quad i, j = 1, \ldots, 6 \tag{43}$$

TABLE 1. Technical specifications of SGE9B06T.

Parameter	Value	Parameter	Value
Rated apparent power (kVA)	2440	Rated frequency (Hz)	90
Rated voltage (V)	1444	Nominal speed (rpm)	1800
Rated current (A)	976	Moment of inertia (kgm^2)	69
Number of poles	6	Power factor	0.95
Connection	⅄		

TABLE 2. The nominal EC parameters of SGE9B06T (Reported by the manufacturer).

Parameter	Value	Parameter	Value
r_s	$6.8365(m\Omega)$	r'_{kd}	$0.1058(m\Omega)$
L_{ls}	$43.315(\mu H)$	L'_{lkd}	$30.1969(\mu H)$
L_{md}	$4.142711(mH)$	r'_{kq}	$0.1273(m\Omega)$
L_{mq}	$1.80035(mH)$	L'_{lkq}	$13.3338(\mu H)$
r'_{fd}	$45.6975(m\Omega)$	L'_{lfd}	$0.1199(H)$

Obviously, if one of the windings of the stator, field, and damper windings is damaged then $r_i(t) > \nu_{Ni}; i = 1, 2, 3$. Also, if $\mathbf{f}_{\mathbf{c}_2}(t) \neq \mathbf{0}_{6\times1}$ and $\mathbf{f}_{\mathbf{c}_1}(t) \neq \mathbf{0}_{6\times1}$, according to (22), the effects of $\mathbf{f}_{\mathbf{c}_1}(t)$ and $\mathbf{f}_{\mathbf{c}_2}(t)$ are added. Clearly, in the presence of the air-gap eccentricity fault or any fault in the stator, field, or damper windings, $r_i(t) > \nu_{Ni}; i = 1, 2, 3$.

Note 2: It is noted that for using $\mathbf{r}(t)$ or calculating $\mathbf{W}$, the state-space model of SGs must be available. In (37), it is assumed that the EC parameters are available. Therefore, $\mathbf{A_c}(\omega_r(t))$, $\mathbf{B_c}$, and $\mathbf{C_c}$ should be determined based on (5b), (5e), and (5f). The nominal EC parameters of SGs are usually available or can be estimated. But it is well known that the actual EC parameters are not equal to the nominal values. In other words, the state-space model of an SG, (5), is an uncertain model. In this condition, the "signal to noise ratio of residual" (**SNRR**) is recommended to be used as an index on the residual vector for fault detection. **SNRR** vector components are defined for each $r_i(t)$ as (44), [10].

$$\mathbf{SNRR} = [SNRR_i]_{n_r\times1} \tag{44a}$$

$$SNRR_i = \left(\int_{t_0}^{t_0+T}\left(r_i^d(t)\right)^2 dt\right) \Big/ \left(\int_{t_1}^{t_1+T}\left(r_i^{FF}(t)\right)^2 dt\right); \quad i = 1,\ldots,n_r \tag{44b}$$

where n_r is the number of residual vector components, $r_i^{FF}(t)$ are the residual vector components from the dataset of the SG in the fault-free condition, and $r_i^d(t)$ are the residual vector components from the dataset of the SG in an unknown condition. T is a user-defined duration. t_1 and t_0 are time instants associated with unknown and fault-free data sequences, respectively. Therefore, fault detection can be done as (45) using **SNRR** components. A flowchart of the introduced fault detection is shown in Figure 2.

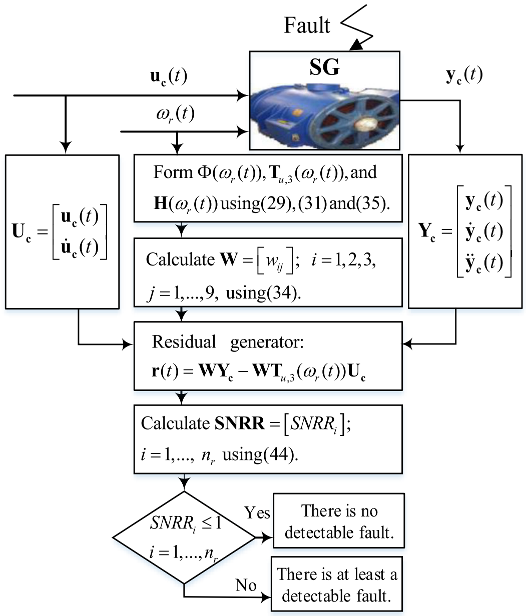

FIGURE 2. Flowchart of the introduced fault detection approach.

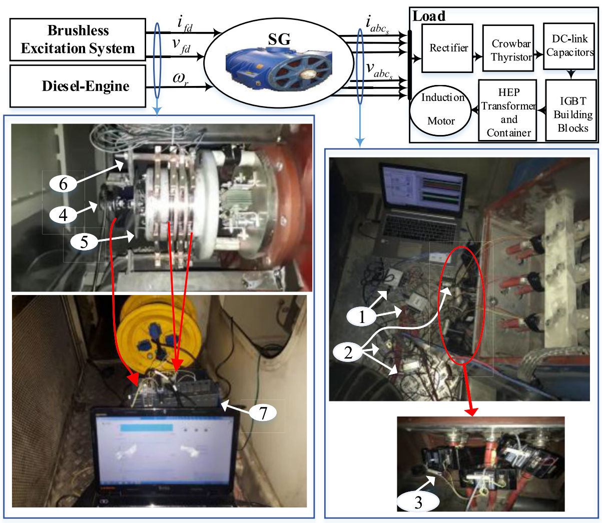

FIGURE 3. A simplified block diagram of the salient-pole SG used in Iran-Safir diesel-electric locomotive and data acquisition system in the 1st SG (HEP: Head End Power, IGBT: Insulated-Gate Bipolar Transistor). 1) NI USB-6009 USB DATA acquisition. 2) Transformer (2000/10). 3) Current transformer (2000/5A). 4) Shaft encoder (100P/R). 5) Slip-ring (contains four rings for measuring field voltage and current). 6) Carbon brush holder. 7) NI cRIO-9025.

$$\begin{cases}\text{If } SNRR_i \le 1; \quad i = 1,\ldots,n_r\\ \text{then there is no detectable fault.}\\ \text{If } SNRR_i > 1; \quad i = 1,\ldots,n_r\\ \text{then there is at least a detectable fault.}\end{cases} \tag{45}$$

Please note that in the constant rotor rotational speed, $\dot{\omega}_r(t) = 0$, the state-space model of SG will be linear.

TABLE 3. The conditions of SGs in each experiment.

Experiment number	SG number	Condition
1st	1	Healthy
2nd	2	
3rd	3	Fault in the field winding (A reduction of the cross-sectional area of wires in the field windings)
4th	4	
5th	5	The air-gap eccentricity fault

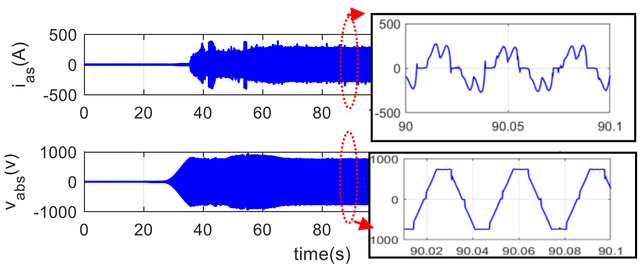

FIGURE 4. The stator line voltage and current for SG number 1 in the healthy condition.

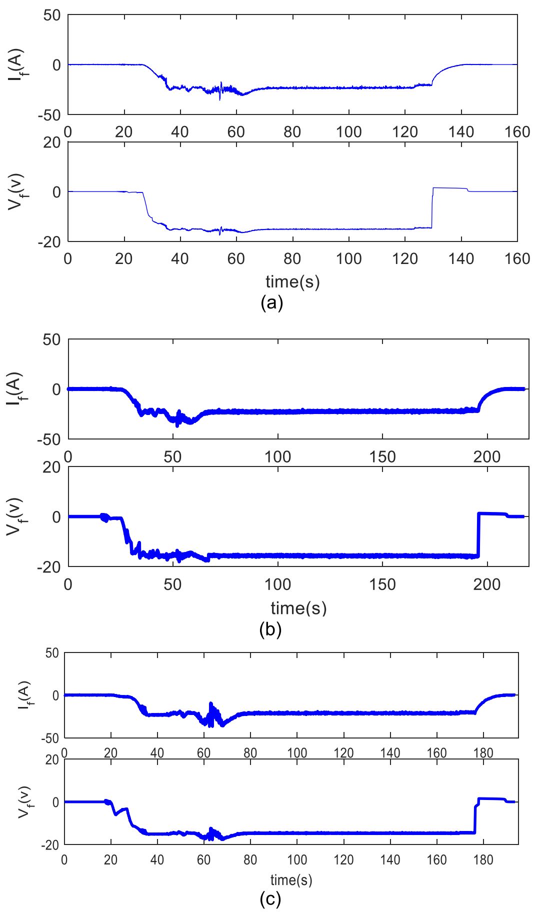

FIGURE 5. Field voltages and currents in the healthy and faulty conditions, (a) SG number 1 in healthy condition, (b) SG number 3 in faulty condition, fault in the field winding, (c) SG number 5 in faulty condition, air-gap eccentricity fault.

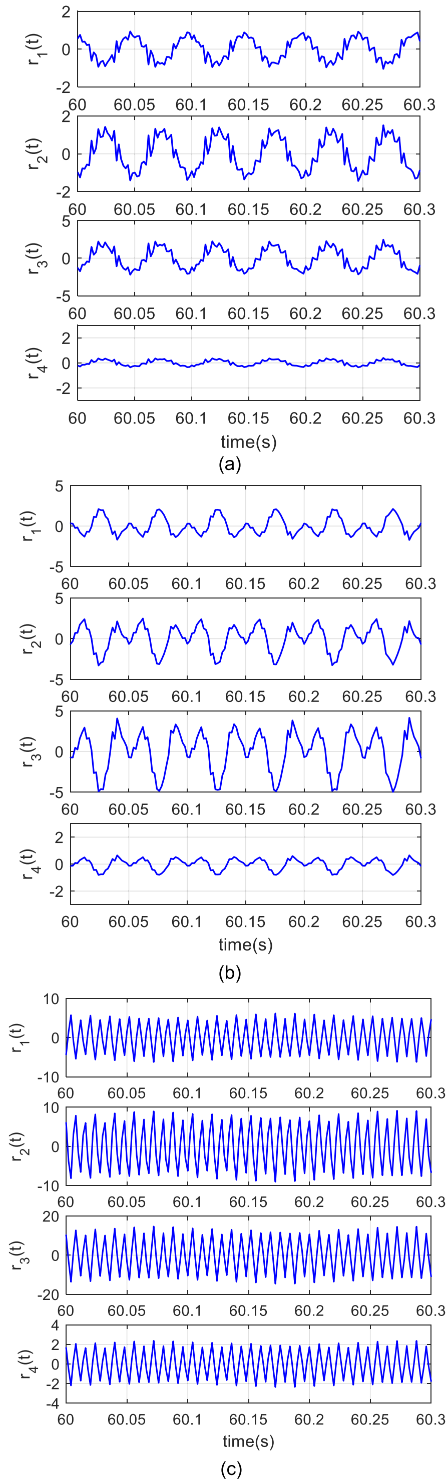

FIGURE 6. Residual vector components in the healthy and faulty conditions: (a) SG number 1 in healthy condition, (b) SG number 3 in faulty condition, fault in the field winding, (c) SG number 5 in faulty condition, air-gap eccentricity fault.

IV. EXPERIMENTAL RESULTS

In order to validate the introduced fault detection approach, appropriate experiments were performed on salient-pole SGs in diesel-electric locomotives. Figure 3 shows a simplified block diagram of the SG and its data acquisition system. The technical specifications and EC parameters of the SG, SGE9B06T, with two damper windings, have been shown in

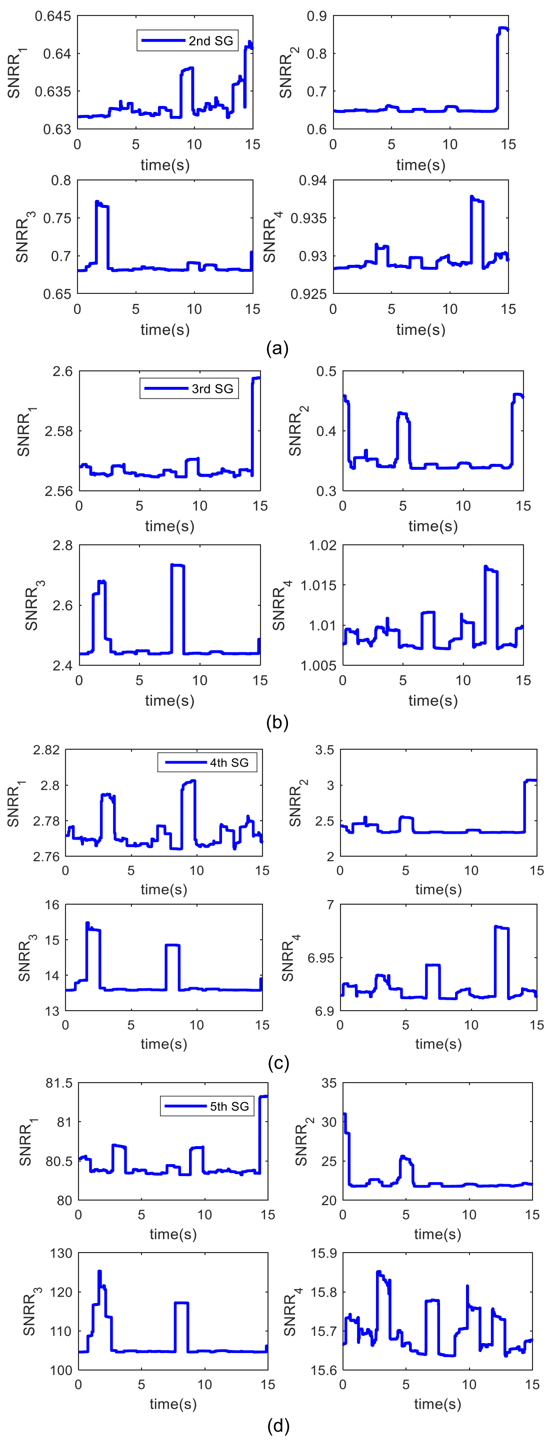

FIGURE 7. SNRR vectors components where the residual vector components from the dataset of SG number 1 were used as $r_i^{FF}(t); i = 1, \ldots, 4$. (a)The residual vector components of SG number 2 as $r_i^d(t); i = 1, \ldots, 4$. (b)The residual vector components of SG number 3 as $r_i^d(t)$. (c) The residual vector components of SG number 4 as $r_i^d(t)$ (d) The residual vector components of SG number 5 as $r_i^d(t)$.

Tables 1 and 2, respectively. Experimental data of the five SGs in five locomotives with nonlinear load in the healthy and faulty conditions were used to demonstrate the effectiveness of the proposed fault detection approach. In all experiments, the rotor rotational speed was constant, $\omega_r(t) = 600.0(RPM)$. The conditions of SGs in each experiment have been presented in Table 3.

In all experiments, data of the line voltages and currents of the stator and field were gathered using two NI-USB 6009 with 5 kHz sampling frequency. Simultaneously, the rotor rotational speed was measured using a shaft encoder and NI cRIO-9025 with 20 kHz sampling frequency. A common signal, field voltage, was recorded using both data loggers to synchronize the recorded data.

Since there are two damper windings in this SG, the order of state-space models of SGs in the healthy and faulty conditions, (5) and (21), are equal to 5 where $n_d = 2$ in (5).

The stator line voltage and current for SG number 1 in the healthy condition and field voltages and currents for SGs numbers 1, 3, and 5 in the healthy and faulty conditions are shown in Figures 4 and 5, respectively. The non-sinusoidal waveforms in Figure 4 show the effect of the nonlinear load. Also, Figure 5 shows that field voltages and currents have no significant differences in the healthy and faulty conditions.

According to (29), (33), and (37), we have $\Phi(\omega_r(t)) \in \mathbf{R}^{9\times5}$, $\mathbf{W} \in \mathbf{R}^{4\times9}$, and $\mathbf{r}(t) = [r_i(t)]_{4\times1}; i = 1, \ldots, 4$. The residual vector components for SGs numbers 1, 3, and 5 in the healthy and faulty conditions at second 60 are shown in Figure 6. The nominal EC parameters are available, we have uncertainty in the state-space model of SGs, (5). Hence, the **SNRR** index based on residual vector is used as (44) -(45) for fault detection in SGs 2 to 5, and their values are shown in Figure 7.

Figure 7, according to (44b), $SNRR_i; i = 1, 2, 3, 4$ are shown by assuming $r_i^{FF}(t) = r_i^1(t)$ where $r_i^1(t); i = 1, \ldots, 4$ are residual vector components, $r_i(t)$, from the dataset of SG number 1. In order to detect a fault in SGs 2 to 5, **SNRR** vectors are calculated using (44), where $r_i^d(t) = r_i^j(t)$ $i = 1, \ldots, 4, j = 2, \ldots, 5$ are residual vector components.

Figure 7 shows the **SNRR** values for SGs 2 to 5. Based on the **SNRR** values in Figure 7, and using (45), we have:

- Figure 7(a): $SNRR_i < 1; i = 1, \ldots, 4$, therefore, there is no detectable fault in SG number 2.
- Figure 7(b): $SNRR_i > 1; i = 1, 3, 4$, therefore, there is a detectable fault in SG number 3.
- Figures 7(c) and 7(d): $SNRR_i > 1; i = 1, \ldots, 4$, therefore, there are detectable faults in the SGs number 4 and 5.

The above results in comparison with the experimental conditions, Table 3, show that the introduced fault detection approach based on **SNRR** analysis is an efficient approach for detecting the SGs faults.

V. CONCLUSION

This paper proposed a model-based fault detection approach based on the residual analysis for SGs by considering two types of faults: (i) a reduction of the cross-sectional area of wires in the field, dampers, and stator windings, and

(ii) air-gap eccentricity. The stator and field currents and voltages, and rotor rotational speed were used for fault detection. The main advantage of the introduced faults detection methodology was its ability to detect both the above faults in the presence of linear and nonlinear loads. By using the experimental results, the validity of the introduced approach was investigated.

REFERENCES

[1] P. C. Krause, O. Wasynczuk, S. D. Sudhoff, and S. Pekarek, *Analysis of Electric Machinery and Drive Systems*, vol. 2. Hoboken, NJ, USA: Wiley, 2002.

[2] N. D. Hatziargyriou, E. S. Karapidakis, G. S. Stavrakakis, I. F. Dimopoulos, and K. Kalaitzakis, ''Identification of synchronous machine parameters using constrained optimization,'' in *Proc. IEEE Porto Power Tech.*, Porto, Portugal, Sep. 2001, p. 5.

[3] L. Liudvinavičius and V. Jastremskas, ''Modernization of diesel-electric locomotive 2M62 and TEP-70 locomotives with respect to electrical subsystem,'' *Proc. Eng.*, vol. 187, pp. 272–280, Jan. 2017.

[4] R. Razavi-Far and M. Kinnaert, ''A multiple observers and dynamic weighting ensembles scheme for diagnosing new class faults in wind turbines,'' *Control Eng. Pract.*, vol. 21, no. 9, pp. 1165–1177, Sep. 2013.

[5] M. Saadat, M. Esfahanian, and M. H. Saket, ''Energy-efficient operation of diesel–electric locomotives using ahead path data,'' *Control Eng. Pract.*, vol. 46, no. 1, pp. 85–93, Jan. 2016.

[6] J. Liu, H. Guo, and Y. Yu, ''Research on the cooperative train control strategy to reduce energy consumption,'' *IEEE Trans. Intell. Transp. Syst.*, vol. 18, no. 5, pp. 1134–1142, Sep. 2016.

[7] M. Kiani, W.-J. Lee, R. Kenarangui, and B. Fahimi, ''Detection of rotor faults in synchronous generators,'' in *Proc. IEEE Int. Symp. Diagnostic Electr. Mach., Power Electron. Drives*, Kraków, Poland, Sep. 2007, pp. 266–271.

[8] M. Mostafaei and J. Faiz, ''An overview of various faults detection methods in synchronous generators,'' *IET Electr. Power Appl.*, vol. 15, no. 4, pp. 391–404, Apr. 2021.

[9] R. Brütsch, M. Tari, K. Fröhlich, T. Weiers, and R. Vogelsang, ''Insulation failure mechanisms of power generators,'' *IEEE Elect. Insul. Mag.*, vol. 24, no. 4, pp. 17–25, Jul./Aug. 2008.

[10] M. Blanke, M. Kinnaert, J. Lunze, M. Staroswiecki, and J. Schröder, *Diagnosis and Fault-Tolerant Control*, vol. 2. Berlin, Germany: Springer, 2006.

[11] J. Faiz, B. M. Ebrahimi, M. Valavi, and H. A. Toliyat, ''Mixed eccentricity fault diagnosis in salient-pole synchronous generator using modified winding function method,'' *Prog. Electromagn. Res. B*, vol. 11, pp. 155–172, 2009.

[12] L. Wang, Y. Li, and J. Li, ''Diagnosis of inter-turn short circuit of synchronous generator rotor winding based on Volterra kernel identification,'' *Energies*, vol. 11, no. 10, p. 2524, Oct. 2018.

[13] N. A. Al-Nuaim and H. A. Toliyat, ''A novel method for modeling dynamic air-gap eccentricity in synchronous machines based on modified winding function theory,'' *IEEE Trans. Energy Convers.*, vol. 13, no. 2, pp. 156–162, Jun. 1998.

[14] I. Tabatabaei, J. Faiz, H. Lesani, and M. Nabavi-Razavi, ''Modeling and simulation of a salient-pole synchronous generator with dynamic eccentricity using modified winding function theory,'' *IEEE Trans. Magn.*, vol. 40, no. 3, pp. 1550–1555, May 2004.

[15] L. Hao, Y. Sun, A. Qiu, and X. Wang, ''Steady-state calculation and online monitoring of interturn short circuit of field windings in synchronous machines,'' *IEEE Trans. Energy Convers.*, vol. 27, no. 1, pp. 128–138, Mar. 2012.

[16] L. Hao, J. Wu, Y. Sun, and X. Wang, ''Simplified mathematical model of inter-turn short circuit of field windings in hydro-generators and its application,'' *Sci. China Technol. Sci.*, vol. 56, no. 4, pp. 898–909, Apr. 2013.

[17] A. Lalami and R. Wamkeue, ''Synchronous generator off-line diagnosis approach including fault detection and estimation of failures on machine parameters,'' *Electr. Power Compon. Syst.*, vol. 41, no. 15, pp. 1501–1517, Nov. 2013.

[18] D. S. Vilchis-Rodriguez and E. Acha, ''A synchronous generator internal fault model based on the voltage-behind-reactance representation,'' *IEEE Trans. Energy Convers.*, vol. 24, no. 1, pp. 184–194, Mar. 2009.

[19] G. Anagnostou, F. Boem, S. Kuenzel, B. C. Pal, and T. Parisini, ''Observer-based anomaly detection of synchronous generators for power systems monitoring,'' *IEEE Trans. Power Syst.*, vol. 33, no. 4, pp. 4228–4237, Jul. 2018.

[20] M. A. Shoaib, A. Q. Khan, G. Mustafa, S. T. Gul, O. Khan, and A. S. Khan, ''A framework for observer-based robust fault detection in nonlinear systems with application to synchronous generators in power systems,'' *IEEE Trans. Power Syst.*, early access, Aug. 24, 2021, doi: 10.1109/TPWRS.2021.3106913.

[21] M. Biet, ''Rotor faults diagnosis using feature selection and nearest neighbors rule: Application to a turbogenerator,'' *IEEE Trans. Ind. Electron.*, vol. 60, no. 9, pp. 4063–4073, Sep. 2013.

[22] C. Bruzzese, ''Diagnosis of eccentric rotor in synchronous machines by analysis of split-phase currents—Part II: Experimental analysis,'' *IEEE Trans. Ind. Electron.*, vol. 61, no. 8, pp. 4206–4216, Aug. 2014.

[23] K. N. Gyftakis, C. A. Platero, Y. Zhang, and S. Bernal, ''Diagnosis of static eccentricity in 3-phase synchronous machines using a pseudo zero-sequence current,'' *Energies*, vol. 12, no. 13, p. 2476, Jun. 2019.

[24] M. Cuevas, R. Romary, J.-P. Lecointe, and T. Jacq, ''Non-invasive detection of rotor short-circuit fault in synchronous machines by analysis of stray magnetic field and frame vibrations,'' *IEEE Trans. Magn.*, vol. 52, no. 7, pp. 1–4, Jul. 2016.

[25] W. Yucai, M. Qianqian, and C. Bochong, ''Fault diagnosis of rotor winding inter-turn short circuit for sensorless synchronous generator through screw,'' *IET Electr. Power Appl.*, vol. 11, no. 8, pp. 1475–1482, Sep. 2017.

[26] C. A. P. Gaona, F. Blázquez, P. Frías, and M. Redondo, ''A novel rotor ground-fault-detection technique for synchronous machines with static excitation,'' *IEEE Trans. Energy Convers.*, vol. 25, no. 4, pp. 965–973, Dec. 2010.

[27] F. R. Blánquez, C. A. Platero, E. Rebollo, and F. Blázquez, ''Field-winding fault detection in synchronous machines with static excitation through frequency response analysis,'' *Int. J. Electr. Power Energy Syst.*, vol. 73, pp. 229–239, Dec. 2015.

[28] M. Pardo, F. R. Blánquez, C. A. Platero, E. Rebollo, and F. Blázquez, ''Detection and location of a ground-fault in the excitation circuit of a 106 MVA synchronous generator by a new on-line method,'' *Electr. Power Syst. Res.*, vol. 140, pp. 303–311, Nov. 2016.

[29] A. Doorwar, B. Bhalja, and O. P. Malik, ''A new internal fault detection and classification technique for synchronous generator,'' *IEEE Trans. Power Del.*, vol. 34, no. 2, pp. 739–749, Apr. 2019.

[30] C. P. Salomon, W. C. Santana, G. Lambert-Torres, L. E. B. da Silva, E. L. Bonaldi, L. E. de Lacerda de Oliveira, J. G. B. da Silva, A. L. Pellicel, G. C. Figueiredo, and M. A. A. Lopes, ''Discrimination of synchronous machines rotor faults in electrical signature analysis based on symmetrical components,'' *IEEE Trans. Ind. Appl.*, vol. 53, no. 3, pp. 3146–3155, May 2017.

[31] M. Kuncan, ''An intelligent approach for bearing fault diagnosis: Combination of 1D-LBP and GRA,'' *IEEE Access*, vol. 8, pp. 137517–137529, 2020.

[32] Y. Zhang, ''Advanced synchronous machine modeling,'' M.S. theses, Dept. Electr. Comput. Eng., Univ. Kentucky, Lexington, KY, USA, 2018.

[33] S. X. Ding, *Model-Based Fault Diagnosis Techniques: Design Schemes, Algorithms, and Tools*. Berlin, Germany: Springer, 2008.

ZAHRA MASOUMI received the B.S. degree in electronic engineering from QIAU, Qazvin, Iran, in 2013, and the M.S. degree in control and signaling engineering from the Control and Signaling Department, School of Railway Engineering, Iran University of Science and Technology, Tehran, Iran, in 2017, where she is currently pursuing the Ph.D. degree.

BIJAN MOAVENI received the B.S. degree in control engineering from the Isfahan University of Technology, Isfahan, Iran, in 2000, and the M.S. and Ph.D. degrees in control engineering from the K. N. Toosi University of Technology, Tehran, Iran, in 2002 and 2007, respectively.

From 2009 to 2015, he was an Assistant Professor and from 2015 to 2018, he was an Associate Professor with the Department of Control and Signaling, School of Railway Engineering, Iran University of Science and Technology, Tehran. Since 2018, he has been an Associate Professor with the Systems and Control Engineering Group, K. N. Toosi University of Technology. He is also a member of the Center of Excellence for Modelling and Control of Complex Systems. He has authored or coauthored more than two books and more than 80 articles. His current research interests include large-scale control systems, control configuration selection, robust control systems, estimation theory, and automatic traffic control systems.

SAYED MOHAMMAD MOUSAVI GAZAFRUDI received the B.S. degree from the University of Shahrood, Iran, in 2001, and the M.Sc. and Ph.D. degrees from the Iran University of Science and Technology, Tehran, Iran, in 2003 and 2009, respectively.

Since 2010, he has been with the School of Railway Engineering, Iran University of Science and Technology, where he is currently an Associate Professor. His current research interests include power quality, renewable energy systems, electric and hybrid vehicles, smart grids, and measurement instrumentation.

JAWAD FAIZ (Senior Member, IEEE) received the bachelor's and master's degrees (Hons.) in electrical engineering from the University of Tabriz, Iran, in 1974 and 1975, respectively, and the Ph.D. degree in electrical engineering from the University of Newcastle upon Tyne, U.K., in 1988. Early in his career, he worked as a Faculty Member with the University of Tabriz for ten years. After obtaining the Ph.D. degree, he rejoined the University of Tabriz, where he held the position of an Assistant Professor, from 1988 to 1992, an Associate Professor, from 1992 to 1997, and has been a Professor, since 1998. Since February 1999, he has been working as a Professor with the Department of Electrical and Computer Engineering, Faculty of Engineering, University of Tehran. His teaching and research interests include switched reluctance and VR motors design and design and modeling of electrical machines and drives. He is a Senior Member of Power Engineering, Industry Applications, Power Electronics, Industrial Electronics, Education, and Magnetics Societies of the IEEE. He is also a member of Iran Academy of Science and Euro-Med Academy of Sciences and Arts.